Journal of the Serbian Society for Computational Mechanics / Vol. 19 / No. 2, 2025 / pp 80-105 / original paper
(10.24874/jsscm.2025.19.02.06)

UNSTEADY MHD NON-NEWTONIAN CASSON FLUID FLOW IN A POROUS MEDIUM WITH CONVECTIVE DIFFUSION, RADIATION, JOULE AND VISCOUS HEATING DISSIPATION EFFECTS: A NUMERICAL STUDY

Bijjula Prabhakar Reddy[1,*] [0000-0002-1776-5064], **Oluwole Daniel Makinde**[2] [0000-0002-3991-4948] **and Paul Majani Matao**[1] [0000-0002-6518-6251]

[1] Department of Mathematics and Statistics, University of Dodoma, P. O. Box 338, Dodoma, Tanzania.
e-mail: prabhakar.bijjula@gmail.com, e-mail: mataopm@yahoo.com
[2] Faculty of Military Science, Saidanha 7395, Private Bag X2, Stellenbosch University, South Africa.
e-mail: makinded@gmail.com
**corresponding author*

Abstract

This article analyzes the behavior of an unsteady mixed convection magneto-hydrodynamic thermo-diffusion and diffusion-thermo flow of heat creating non-Newtonian Casson fluid flow from an exponentially stimulating vertical porous plate encased in porous structure. The flow of fluid is caused by a ramped form temperature and concentration. In addition to this, chemical reaction, radiation, Joule and viscous heating dissipation effects are also integrated in the given problem. The coupled, nonlinear, non-dimensional governed model equations are resolved numerically by accepting the finite difference scheme. Computational results evidencing the comportment of the velocity, temperature and concentration profiles to the emerging parameters variation are displayed via graphical representations whereas the skin-friction, Sherwood and the Nusselt numbers are displayed via tables. The ensuing outcomes exposed that viscous heating dissipation, heat genesis, thermal radiation and diffusion thermo effects intensify the Casson fluid velocity and temperature. Likewise, the porosity parameter and buoyancy effects amplify the fluid velocity, but a contrary aspect is noted in consequence of the Casson parameter and magnetic potency. The fluid motion and concentration upgrade due to the thermo-diffusion effect, whereas the reverse anomaly is reported due to the chemical reaction aspect. Also, reduction is traced in the Nusselt number and skin-friction for greater viscous dissipation, Dufour effect and heat-producing parameter.

Keywords: MHD, chemical reaction, Soret-Dufour effect, Casson fluid, viscous dissipation, heat generation.

1. Introduction

Fluids can be discriminated by the use of Newton's viscosity rule that defines the shear stress is directly proportional to shear stress rate for Newtonian and non-Newtonian fluids. The fluid that

does not satisfy Newton's viscosity rationale is called a non-Newtonian fluid. Casson fluids belong to the non-Newtonian liquid category and can describe the control of viscous force owing to capricious viscosity. Examples of such liquids are honey, jelly, concentrated fruit juices, tomato sauce, human blood, paints, etc. The investigation of non-Newtonian Casson fluid has enlisted inspection of the vast number of researchers on the environs as things go to its compelling utilization in the areas of bio-engineering operations, juice synthesis, drilling operations, metallurgy, food processing, together with the manufacturing of pharmaceutical products. The modeling of non-Newtonian Casson fluid problems brings out the differential equations, which are more arduous due to the higher order than that of the Navier–Stoke's equations. Consequently, obtaining the exact analytical solutions to these equations is an adversity. Amongst plenteous models of the non-Newtonian fluid, Casson's fluid model is the trendiest one, also termed the "rheological model" initially; it was illustrated by Casson (1959). Many research investigations, such as those by Hussanan et al. (2014), Khalid et al. (2015a), Khalid et al. (2015b), Das et al. (2015), Kataria and Patel (2016a), Kataria and Patel (2016b), Mohamed et al. (2017), Hussanan et al. (2017), Kataria and Patel (2018) and Karatia and Patel (2019), explained the Casson fluid deportment in the boundary layer under diverse geometrical configurations. The performance of MHD non-Newtonian Casson fluid with distinct plate surfaces was interpreted in consideration of divergent boundary specifications by Das et al. (2019) and Endalew (2021).

The far-reaching results of the MHD radiating and reacting heat and mass transmission problem have captivated several researchers on the grounds that its extensive array of immense implementations in distinguishing scientific, engineering and industry expansion, such as the high-temperature casting, gas turbines, nuclear power plants, food processing, catalytic chemical reactors, thermo-nuclear amalgam, power genesis systems, petroleum and chemical management, solar power, photo-ionization, missiles, unusual-temperature plasmas, actuation devices for aircraft, tabular reactors, oxidation of solid deposition and incorporation of ceramic materials. The investigators Prabhakar Reddy and Anand Rao (2011), Venkateshwarlu et al. (2013), Seth et al. (2015), Prabhakar Reddy (2019), Veeresh et al. (2019) and Patel (2019) researched the consequences of radiation and chemical reactivity on different MHD fluids moving under discreet circumstances. In continuation, Shamshuddin et al. (2019) numerically discussed the radiative Casson reacting fluid moving above the inclined plate. Rajput et al. (2020) scrutinized non-Newtonian thermo-solutal convective Casson radiative fluid conveyance with heat source/sink enlightened by Arrhenius kinetics over a vertical plate. Nandi and Kumbhakar (2021) conferred analytically hydro-magnetic oscillatory flow of radiative and reactive flow admitting ramped temperature and ramped concentration. Prabhakar Reddy and Makinde (2021) and Prabhakar Reddy and Makinde (2022) recently analyzed the influence of chemical reaction on radiating MHD flow under different fluid flow patterns.

The flow field is constrained by density imbalance when coupled heat and mass diffusion exist simultaneously in diversified industrial developments. Newtonian heating, mass balances and concentration gradients amplify density imbalances. The thermo-diffusion (Soret) response is the mass transition, because of the temperature alteration, although the diffusion-thermo (Dufour) effect is its reversion. The Soret-Dufour effect is of second-order occurrence and is momentous in geosciences, petrology and hydrology. These effects are significantly used for isotope separation of gases surrounded by medium molecular weight substances such as nitrogen gas and air, for mixing with very-light molecular weighted gases such as hydrogen, helium etc. Considering these significant applications, the investigations Sudhakar and Gangadhar (2012), EI-Kabeir et al. (2013), Pal et al. (2016), Hayat et al. (2016), Sreedevi et al. (2017), Prabhakar Reddy and Sunzu (2018) effectively explored the Soret-Dufour effect by considering different fluids with dissimilar surface conditions. Subsequently, Hayat et al. (2018) discussed Soret-Dufour's effect on the peristaltic MHD Prandtl liquid flow through the rotating system. Kaladhar

et al. (2019) investigated Soret-Dufour impacts in reacting mixed convection fluid passing through annulus by considering Navier slip and convective boundary situations.

When the fluid is sufficiently viscous, it is essential to take into account the viscous dissipation's effect in heat transfer investigation. Moreover, influential applications of the viscous dissipation impacts are found in polymer manufacturing, instrumentation, food processing, tribology, lubrication, etc. Thus, specific outstanding research works have been presented due to these significant applications. The researchers Pal et al. (2014), Singh and Kumar (2016), Prabhakar Reddy (2016), Gopal et al. (2017), Shamshuddin and Tirupathi (2017), Ibrahim et al. (2017), Reddy et al. (2018), Shamshuddin et al. (2018) and Seth et al. (2019) inspected viscous dissipation effects by considering different fluids, namely micro-polar fluid, nanofluid, Casson fluid and Oldroyd-B fluid for dissimilar circumstances. Subsequently, Ullah et al. (2019) addressed the chemical reactive heat dissipation slip flow of MHD Casson fluid in the instance of heat generation/heat immersion over a nonlinear porous stretching cylinder. Then, Ferdows et al. (2020) deliberated dissipative micro-polar radiating fluid flow with cross-diffusion consequences in a non-Darcy porous surround. Recently, Prabhakar Reddy and Joseph (2022) looked into the heat captivating MHD Casson dissipating fluid passing across an oscillating vertical permeable surface in consideration of Newtonian heating effect.

Motivated by the above intensive literature interpretation, the current numerical inspection delves into the radiative and reactive unsteady mixed convection magneto-hydrodynamic thermo-diffusion and diffusion-thermo flow of heat producing non-Newtonian Casson fluid from an exponentially stimulating vertical porous surface with ramp system surface temperature and concentration, as this study is lacking in the available literature. During the stringent literature overview of already published works, authors ascertained that the works by Khalid et al. (2015a), Hussanan et al. (2017) and Kataria and Patel (2018) and Kataria and Patel (2019) considered the Casson fluid but didn't consider the Casson parameter aspect in the permeability of the porous medium. Additionally, the term seeming for the heating dissipation by cause of porous permeability was overlooked by the studies Gopal et al. (2017) and Reddy et al. (2018). Hence, in the commenced investigation, we have integrated mentioned missing effects on the flow field, so that the results of the expected research are novel. Governing equations of the intended model are nonlinear coupled PDEs which can be resolved by finite difference numerical scheme. The relevant results are exemplified by graphical representations and tables and are studiously discussed. A comparative study is conveyed to verify the accuracy and exactness of the study's findings with earlier published works in the literature affirm excellent agreement.

2. Model depiction

Consider a mixed convection unsteady 2D MHD heat emanating non-Newtonian Casson fluid hastening from an exponentially escalating vertical porous plate placed in a porous material with ramp form concentration and temperature. The plate is being stationed at $y' = 0$, with $x'-$axis is leading the plate in a vertical direction, fluid transversal is being defined to $y' > 0$, and y'axis normally to the plate surface is outlined in Fig.1. The Soret impression is the heat flux induced by temperature intensity and Dufour impression is reciprocate of it and both aspects have been comprised in the study. The fluid tinctured by a consistent magnetic potency B_0 applied in $y'-$ direction. The chemical reaction component $K_c^{'}$ of order one is treated amidst the fluid and dispersing species. Initially, the plate and fluid are pretended at the persistent temperature $T_\infty^{'}$ and surface concentration $C_\infty^{'}$, respectively. For $t' > 0$, the plate with tempo $u_0 e^{(a't')}$ is exponentially accelerating in its plane. Accompanying temperature and species concentration of

the fluid is either upraised or dropped, into $T_\infty^{'}+(T_w^{'}-T_\infty^{'})(t'/t_0)$ and $C_\infty^{'}+(C_w^{'}-C_\infty^{'})(t'/t_0)$ for $t'\le t_0$ and for $t'>t_0$, maintained constants $T_w^{'}$ and $C_w^{'}$, respectively. The importance of the magnetic sway is not used in the current research since the fluid Reynolds number is small. Likewise, import of polarization of charges is excluded because there is no external electric field. For an isotropic and incompressible Casson fluid stream, the rheological equation of state for the Cauchy stress tensor is as follows (Kalid et al. (2015a) and Hussanan et al. (2017));

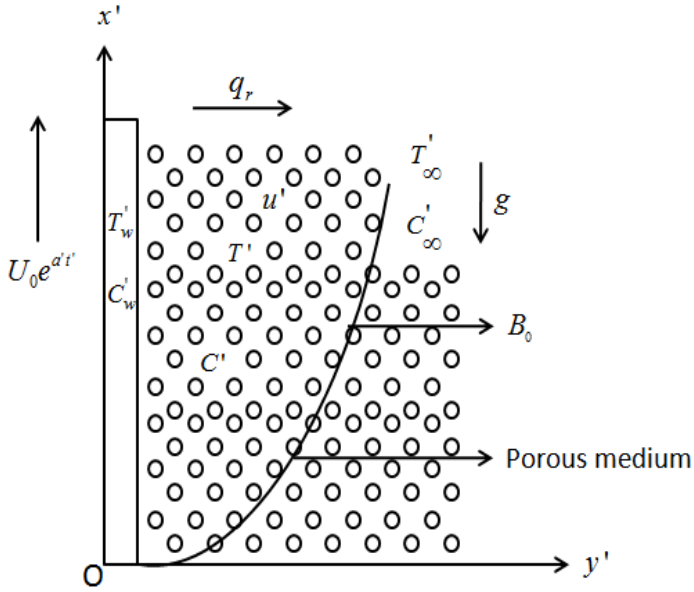

Fig.1. Physical sketch of the problem.

$$\tau_{ij}=\begin{cases}2(\mu_B+\dfrac{p_y}{\sqrt{2\pi}})e_{ij} & \text{when } \pi>\pi_c\\ 2(\mu_B+\dfrac{p_y}{\sqrt{2\pi_c}})e_{ij} & \text{when } \pi<\pi_c\end{cases} \tag{1}$$

In Eq. (1), $\pi=(e_{ij})(e_{ij})$ where e_{ij} stands for $(i,j)^{th}$ component of deformation strain rate tensor, μ_B – stands for the plastic dynamical viscosity, p_y – stands for the fluid's yield stress, π – stands for the product of deformation components, and π_c – stands for the crucial condition of the product on the non-Newtonian fluid. When $\pi<\pi_c$, we realized from Eq. (1)

$$\tau_{ij}=2\mu_B\left(1+\frac{1}{\beta}\right)e_{ij} \tag{2}$$

In Eq. (2), $\beta=\mu_B\sqrt{2\pi_c}\,/\,p_y$ is the Casson fluid parameter. As $\beta\to\infty$, the existence of non-Newtonian fluid vanishes and acts similar to the Newtonian fluid. By taking the

abovementioned interpretation with facilitate of the Boussinesq's estimation, the flow controlling equations of the physical phenomena with matching initial and boundary conditions:

$$\frac{\partial u'}{\partial t'} = \upsilon\left(1+\frac{1}{\beta}\right)\frac{\partial^2 u'}{\partial y'^2} - \frac{\sigma B_0^2}{\rho}u' - \left(1+\frac{1}{\beta}\right)\frac{\upsilon\varphi}{K_p'}u' + g\beta^t\left(T'-T_\infty'\right) + g\beta^c\left(C'-C_\infty'\right) \tag{3}$$

$$\begin{aligned}\frac{\partial T'}{\partial t'} = {} & \frac{k_t}{\rho c_p}\frac{\partial^2 T'}{\partial y'^2} - \frac{1}{\rho c_p}\frac{\partial q_r}{\partial y'} + \frac{D_m k_T}{c_s c_p}\frac{\partial^2 C'}{\partial y'^2} + \frac{Q_H}{\rho c_p}(T'-T_\infty') + \frac{\upsilon}{c_p}\left(1+\frac{1}{\beta}\right)\left(\frac{\partial u'}{\partial y'}\right)^2 \\ & + \frac{\sigma B_0^2}{\rho c_p}u'^2 + \left(1+\frac{1}{\beta}\right)\frac{\upsilon\varphi}{K_p'}u'^2\end{aligned} \tag{4}$$

$$\frac{\partial C'}{\partial t'} = D_m\frac{\partial^2 C'}{\partial y'^2} + \frac{D_m k_T}{T_m}\left(\frac{\partial^2 T'}{\partial y'^2}\right) - K_c'(C'-C_\infty') \tag{5}$$

Here, u', ρ, B_0, β^t, T', Q_H, g, t', φ, C', c_p, k_T, σ, K_c', q_r, T_m, K_p', c_s, D_m, k_T, β^c and υ, respectively denote the fluid velocity, fluid density, uniform magnetic field strength, thermal expansion constant, fluid temperature, heat generation coefficient, acceleration by cause of gravity, time, porosity of the medium, fluid concentration, specific heat at a consistent pressure, thermal diffusion rate, electrical conductivity, chemical reaction coefficient, radiation heat alter, mean fluid temperature, permeability parameter, concentration susceptibility, molecular mass diffusivity, thermal conductivity, solute expansion constant and the kinematic viscosity.

$$u' = 0,\ T' = T_\infty',\ C' = C_\infty' \qquad \text{for } y' \geq 0 \text{ when } t' \leq 0 \tag{6a}$$

$$u' = u_0 e^{(a't')} \qquad \text{at } y' = 0 \text{ when } t' > 0 \tag{6b}$$

$$\begin{cases} T' = T_\infty' + (T_w' - T_\infty')t'/t_0 & \text{at } y' = 0 \text{ when } 0 < t' \leq t_0 \\ T' = T_w' & \text{at } y' = 0 \text{ when } t' > t_0 \end{cases} \tag{6c}$$

$$\begin{cases} C' = C_\infty' + (C_w' - C_\infty')t'/t_0 & \text{at } y' = 0 \text{ when } 0 < t' \leq t_0 \\ C' = C_w' & \text{at } y' = 0 \text{ when } t' > t_0 \end{cases} \tag{6d}$$

$$u' \to 0,\ T' \to T_\infty',\ C' \to C_\infty' \quad \text{as } y' \to \infty \text{ when } t' > 0 \tag{6e}$$

By making use of the Rosseland diffusion approximate [46], the radiative heat variability vector q_r endowed to:

$$q_r = -\frac{4\sigma_S}{3k_m}\frac{\partial T'^4}{\partial y'} \tag{7}$$

Here, σ_S and k_m, respectively the Stefan-Boltzmann mean captivation constants. By assuming the temperature deviation in the flow region appropriately meager, we elaborate T'^4 by Taylor's series around T_∞', then dropping from 2nd term onwards in the resulting series imparts

$$T'^4 \cong 4T_\infty'^3 T' - 3T_\infty'^4 \tag{8}$$

Using Eq. (8) into Eq. (7) yields

$$\frac{\partial q_r}{\partial y'} = -\frac{16\sigma_s T'^3_\infty}{3k_m}\left(\frac{\partial^2 T'}{\partial y'^2}\right) \tag{9}$$

Substituting Eq. (9) into energy Eq. (4) gives away

$$\begin{aligned}\frac{\partial T'}{\partial t'} = &\left(\frac{k_t}{\rho c_p} + \frac{16\sigma_S T'^3_\infty}{3k_m \rho c_p}\right)\frac{\partial^2 T'}{\partial y'^2} + \frac{Q_H}{\rho c_p}(T' - T'_\infty) + \frac{\upsilon}{c_p}\left(1+\frac{1}{\beta}\right)\left(\frac{\partial u'}{\partial y'}\right)^2 + \frac{\sigma B_0^2}{\rho c_p}u'^2 \\ &+\left(1+\frac{1}{\beta}\right)\frac{\upsilon\varphi}{K'_p}u'^2 + \frac{D_m k_T}{c_s c_p}\left(\frac{\partial^2 C'}{\partial y'^2}\right)\end{aligned} \tag{10}$$

We define the specified dimensionless physical parameters and quantities:

$$\left.\begin{aligned}&\xi = \frac{y'}{t_0 u_0},\ \tau = \frac{t'}{t_0},\ t_0 = \frac{\upsilon}{u_0^2},\ u = \frac{u'}{u_0},\ P_r = \frac{\upsilon\rho c_p}{k_t},\ M^2 = \frac{\sigma B_0^2 \upsilon}{\rho u_0^2},\ a = \frac{a'\upsilon}{u_0^2},\\ &S_c = \frac{\upsilon}{D_M}, N_r = \frac{16\sigma_S T'^3_\infty}{3k_t k_m},\ \theta = \frac{(T' - T'_w)}{(T'_w - T'_\infty)},\ C = \frac{(C' - C'_w)}{(C'_w - C'_\infty)},\ K_c = \frac{\upsilon K'_c}{u_0^2},\\ &K = \frac{K'_p u_0^2}{\upsilon\varphi},\ S_r = \frac{D_m k_T (T'_w - T'_\infty)}{\upsilon T_m (C'_w - C'_\infty)},\ E_c = \frac{u_0^2}{c_p (T'_w - T'_\infty)},\ D_u = \frac{D_m k_T (C'_w - C'_\infty)}{c_s c_p (T'_w - T'_\infty)},\\ &H = \frac{Q_H \upsilon}{u_0^2 \rho c_p},\ G_r = \frac{\beta^t \upsilon g (T'_w - T'_\infty)_\infty}{u_0^3},\ G_m = \frac{\beta^c \upsilon g (C'_w - C'_\infty)}{u_0^3}.\end{aligned}\right\} \tag{11}$$

Using Eq. (11), into Eqs. (3), (5), (6a – 6e) and (10) admits the dimensionless flow restricted PDEs of the physical procedure:

$$\frac{\partial u}{\partial \tau} = \left(1+\frac{1}{\beta}\right)\frac{\partial^2 u}{\partial \xi^2} - \left[M^2 + \left(1+\frac{1}{\beta}\right)\frac{1}{K_p}\right]u + G_r\theta + G_m C \tag{12}$$

$$\frac{\partial \theta}{\partial \tau} = \frac{(1+N_r)}{P_r}\frac{\partial^2 \theta}{\partial \xi^2} + D_u\left(\frac{\partial^2 C}{\partial \xi^2}\right) + E_c\left(1+\frac{1}{\beta}\right)\left(\frac{\partial u}{\partial \xi}\right)^2 + E_c\left[M^2 + \frac{1}{K_p}\left(1+\frac{1}{\beta}\right)\right]u^2 + H_s\theta \tag{13}$$

$$\frac{\partial C}{\partial \tau} = \frac{1}{S_c}\frac{\partial^2 C}{\partial \xi^2} + S_r\left(\frac{\partial^2 \theta}{\partial \xi^2}\right) - K_c C \tag{14}$$

Here, ξ, τ, G_m, S_c, G_r, u, K_p, β, M, a, θ, N_r, D_u, H_s, E_c, S_r and K_c, respectively denote the span-wise coordinate, time, mass Grashof number, Schmidt number, thermal Grashof number, dimensionless velocity, permeability parameter, Casson parameter, magnetic intensity, acceleration parameter, dimensionless temperature, radiation parameter, Dufour parameter, heat-generated parameter, Eckert parameter, and the chemical reaction factor.

The initial and boundary specified by (6a) – (6e), turn into

$$u = 0,\ \theta = 0,\ \mathrm{C} = 0 \qquad \text{for } \xi \geq 0 \text{ when } \tau \leq 0 \tag{15a}$$

$$u = e^{(a\tau)} \qquad \text{at } \xi = 0 \text{ when } \tau > 0 \tag{15b}$$

$$\theta = \begin{cases} \tau & \text{at } \xi = 0 \text{ when } 0 < \tau \le 1 \\ 1 & \text{at } \xi = 0 \text{ when } \tau > 1 \end{cases} \tag{15c}$$

$$C = \begin{cases} \tau & \text{at } \xi = 0 \text{ when } 0 < \tau \le 1 \\ 1 & \text{at } \xi = 0 \text{ when } \tau > 1 \end{cases} \tag{15d}$$

$$u \to 0,\ \theta \to 0,\ C \to 0 \quad \text{as } \xi \to \infty \text{ when } \tau > 0 \tag{15e}$$

The physical quantities important in engineering, the dimensionless skin-friction, Nusselt and Sherwood numbers at the plate surface, respectively are defined by

$$S_f = -\left(1+\frac{1}{\beta}\right)\left(\frac{\partial u}{\partial \xi}\right)_{\xi=0},\ N_u = -(1+N_r)\left(\frac{\partial \theta}{\partial \xi}\right)_{\xi=0} \text{ and } S_h = -\left(\frac{\partial C}{\partial \xi}\right)_{\xi=0}$$

3. Computational procedure

The governing Eqs. (12) – (14) of the model are nonlinear coupled partial differential equations, for which the exact solutions are almost impossible, so we must utilize a numerical scheme. Hence, the explicit finite difference scheme is used to simplify the governing equations, which is simple, accurate and effective. By using the forward time and central difference in space for u, θ and C, the finite difference form of Eqs. (12) – (14) is given by

$$\left.\begin{aligned} u_j^{k+1} = u_j^k + \left(1+\frac{1}{\beta}\right)\left(\frac{\Delta\tau}{\Delta\xi^2}\right)\left(u_{j-1}^k - 2u_j^k + u_{j+1}^k\right) - (\Delta\tau)\left(u_j^k\right)\left(M^2 + \left(1+\frac{1}{\beta}\right)\frac{1}{K_p}\right) \\ + (\Delta\tau)\left(G_r\theta_j^k + G_m C_j^k\right) \end{aligned}\right\} \tag{16}$$

$$\left.\begin{aligned} \theta_j^{k+1} = \theta_j^k + \left(\frac{1+N_r}{P_r}\right)\left(\frac{\Delta\tau}{\Delta\xi^2}\right)\left(\theta_{j-1}^k - 2\theta_j^k + \theta_{j+1}^k\right) + (D_u)\left(\frac{\Delta\tau}{\Delta\xi^2}\right)\left(C_{j-1}^k - 2C_j^k + C_{j+1}^k\right) \\ + (\Delta\tau)(H_s)\left(\theta_j^k\right) + \frac{E_c}{(2\Delta\xi)^2}(\Delta\tau)\left(1+\frac{1}{\beta}\right)\left(u_{j+1}^k - u_{j-1}^k\right)^2 \\ + (\Delta\tau)E_c\left[M^2 + \frac{1}{K_p}\left(1+\frac{1}{\beta}\right)\right]\left(u_j^k\right)^2 \end{aligned}\right\} \tag{17}$$

$$\left.\begin{aligned} C_j^{k+1} = C_j^k + \left(\frac{1}{S_c}\right)\left(\frac{\Delta\tau}{\Delta\xi^2}\right)\left(C_{j-1}^k - 2C_j^k + C_{j+1}^k\right) \\ + (S_r)\left(\frac{\Delta\tau}{\Delta\xi^2}\right)\left(\theta_{j-1}^k - 2\theta_j^k + \theta_{j+1}^k\right) - (\Delta\tau)(K_c)C_j^k \end{aligned}\right\} \tag{18}$$

Eqs. (15*a* – 15*e*) in the finite difference form can be displayed as follows:

$$u_j^k = 0,\ T_j^k = 0,\ \mathrm{C}_j^k = 0 \qquad \text{for all } j \text{ and } k \tag{19a}$$

$$u_j^k = U_0 e^{a\tau} \qquad \text{at } j=0 \text{ for } k>0 \tag{19b}$$

$$\theta_j^k = \begin{cases} \tau & \text{at } j=0 \text{ and } 0<k\le 1 \\ 1 & \text{at } j=0 \text{ for } k>1 \end{cases} \tag{19c}$$

$$C_j^k = \begin{cases} \tau & \text{at } j=0 \text{ and } 0<k\le 1 \\ 1 & \text{at } j=0 \text{ for } k>1 \end{cases} \tag{19d}$$

$$u_j^k \to 0,\ \theta_j^k \to 0,\ C_j^k \to 0 \qquad \text{as } j\to\infty \text{ for } k>0 \tag{19e}$$

The indices in the above equations, j and k denote the space ξ and time τ, $\Delta\xi$ and $\Delta\tau$ denote grid dimensions in ξ and $\tau-$directions, respectively. The values of flow fields such as u, θ and C are known at $\tau=0$. Then velocity, temperature and concentration fields are at time $\tau_{k+1}=\tau_k+\Delta\tau$ by accepting the noted values of the preceding time $\tau=\tau_k$ for all $k=0,1,2,...N-1$. These processes are reiterated to reach the convergent solution for velocity, temperature and concentration fields. Finally, the grid size is fixed at $\Delta\tau=0.01$ and $\Delta\xi=0.005$ for the whole computational process to ensure the stability and convergence. The verification of the code accuracy is done by making the comparison.

3.1 Code verification

To establish the precision of our endowed results and adopted numerical technique in this problem, we have conducted a comparison in the particular cases of the current findings with those of analytical results already published by Kataria and Patel (2019) and Nandi and Kumbhakar (2021) by reckoning the Nusselt number N_u. It is very much clear-cut from Tables 1 and 2, that our results are in splendid accordance when $N_r=0,\ D_u=0$ and $E_c=0$, with the results of Kataria and Patel (2019) and when $P_r=0.71,\ D_u=0$ and $E_c=0$, with the results of Nandi and Kumbhakar (2021), respectively. Therefore, presented results in this research are accurate.

P_r	$-H$	τ	Kataria and Patel (2019)		FDM results	
			Ramped	Isothermal	Ramped	Isothermal
15	3	0.4	3.7563	6.9349	3.756348	6.934998
16			3.8795	7.1623	3.879761	7.162351
17			3.9989	7.3827	3.998906	7.382528
15	2		3.4481	5.9019	3.448093	5.901971
	1		3.1185	4.7517	3.118554	4.751808
	3	0.5	4.4445	6.8392	4.444500	6.839229
		0.6	5.1256	6.7869	5.125691	6.786187

Table 1. A comparison study of N_u at $N_r=0,\ D_u=0$ and $E_c=0$.

H_s	N_r	τ	Nandi and Kumbhakar (2021)		FDM results	
			Ramped	Isothermal	Ramped	Isothermal
3	2	0.2	0.19317	0.20373	0.193172	0.203736
1			0.22879	0.48672	0.228799	0.486722
4			0.17412	0.04510	0.174125	0.045104
3	6		0.12646	0.13337	0.126463	0.133370
	10		0.10088	0.10369	0.100880	0.103695
	2	0.1	0.15569	0.59372	0.155694	0.593727
		0.15	0.17918	0.36352	0.179181	0.363522

Table 2. A comparison study of N_u at $P_r = 0.71$, $D_u = 0$ and $E_c = 0$.

4. Analysis of graphical results

To emphasize the propensity of the Casson fluid velocity, temperature and concentration on account of diversified flow-controlled parameters such as H_s, K_c, S_r, N_r, G_r, K_p, D_u, E_c, β, G_m, M, a and τ, we have computed numerical values for u, θ and C and these collected numerical results were sketched in figures 2-22 versus boundary layer coordinate ξ for two thermal conditions. The numerical variance of the skin-friction, Nusselt and the Sherwood numbers are demonstrated through the Tables 3-5 for two thermal conditions.

Figures 2 and 10 are drawn to describe the variance of fluid temperature and velocity for dissimilar heat-generated parameter H_s, respectively. We observe a growth in both fluid temperature and velocity with augmentation of H_s, which is a physical reality. Because of extending values H_s carries extra heat source affords higher thermal energy, which enhances fluid temperature and consequently quickens fluid flow. Figures 3 and 11 were sketched to emphasize the variation of the fluid temperature and velocity against the Eckert number E_c. These figures show that both temperature and velocity augmented on enriching values of E_c. This can be attributed to the fact that, for greater E_c values material particles become extra energetic because of huge amount of energy deposit in the flow regime causes to improve the fluid temperature, eventually intensify the flow velocity. Figures 4 and 12 display the variation of fluid temperature and velocity due to the increase of radiation parameter N_r. These figures demonstrate that the fluid temperature as well fluid velocity upsurges on increasing radiation parameter. Physically, increasing N_r produce extra heat dispersion inside the boundary layer as a consequence enhance the fluid temperature, ultimately accelerate the flow velocity. Figures 5 and 13 are plotted to investigate the effect of diffusion-thermo parameter D_u on the temperature and velocity profiles, respectively. The fluid temperature and velocity increases with the swelling Dufour parameter. Figures 7 and 14 summarize the alteration of fluid concentration and velocity for dissimilar chemical reaction parameter K_c. These plots admit that the velocity as well concentration distributions diminish within the boundary layer for ascending values of K_c. To be more specific, we have chosen the instance of a destructive chemical reaction ($K_c > 0$). It is significant to note that an enlargement of K_c results in the reduction of species concentration inside the boundary-layer which causes to deteriorate concentration distribution, in due course

decelerate fluid velocity. Figs. 8 and 15 were sketched to capture the influence of the thermo-diffusion parameter S_r on the fluid concentration and velocity, respectively. From these figures, we ascertained a considerable growth in the fluid concentration and velocity with rising thermo-diffusion parameter. The physics behind this result is that when S_r increases, width of concentration boundary layer expands due to the higher thermal gradient resulting in an appreciable increase of fluid concentration, consequently speed-up the fluid velocity. Figures 16 and 17 elucidate the effects of buoyant strengths G_r and G_m, respectively on the velocity profiles. Attention is focused on $G_r > 0$, which specifies that the plate cooling problem and $G_m > 0$, which specifies that the species of chemical reaction in the free stream state is lesser to that of boundary surface. It is confirmed from these plots that altering values of G_r and G_m the fluid velocity amplified in the boundary layer. Since G_r and G_m signifies the relative strengths of thermal and solutal buoyancy forces to viscous force, respectively. The physical logic behind this result is that increasing G_r and G_m leading to intensify the thermal and solutal buoyancy strengths consequently speed-up the fluid velocity across the boundary layer regime. The variation of the fluid velocity is depicted in Figure 18 due to the alteration of magnetic field M. It is detected a significant decrement in the fluid movement with ascending values of M, which is physically acceptable. This decreasing trend in the flow is due to the magnetic influence on the flow region, developing a delaying body exaction termed “Lorenz force” that decreases the fluid velocity. The opposite effect is identified in the fluid velocity with an increase of porosity parameter K_p, which is seen in Fig. 19. Physically, increased values of K_p causes larger voids in a porous medium; we consequently have increased flow in the medium. The effect of the Casson parameter β on the fluid velocity is discussed in Fig.20. It was shown that there is deterioration in the fluid momentum for higher values of β. As a matter of fact, higher values of β deteriorate yield stress, resulting in the improvement of plastic dynamic viscosity, thus diminish fluid velocity. Figure 21 shows the impact of acceleration parameter a on the velocity profiles. This diagram indicates that ascending acceleration parameter causes higher fluid velocity. It is realized from Figures 6, 9 and 22 that the fluid temperature, concentration and velocity increases with the time τ. These results for temperature, concentration and velocity curves correspond to the specified initial and boundary conditions Eq. $(15a)-(15e)$.

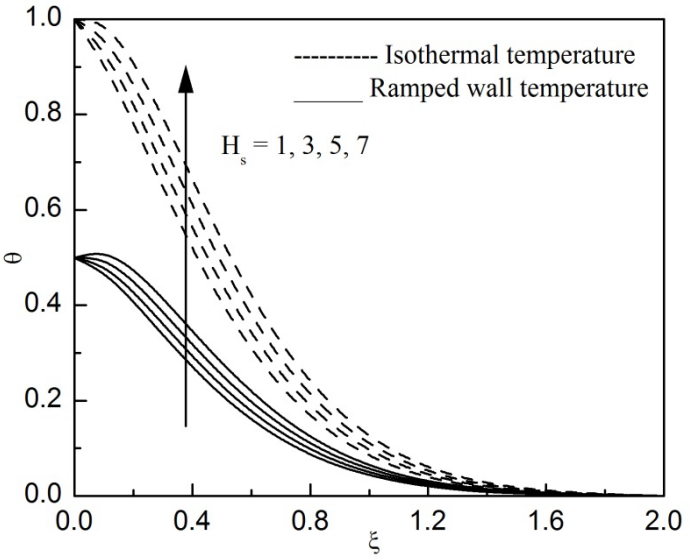

Fig.2. Temperature vs ξ for several H_s.

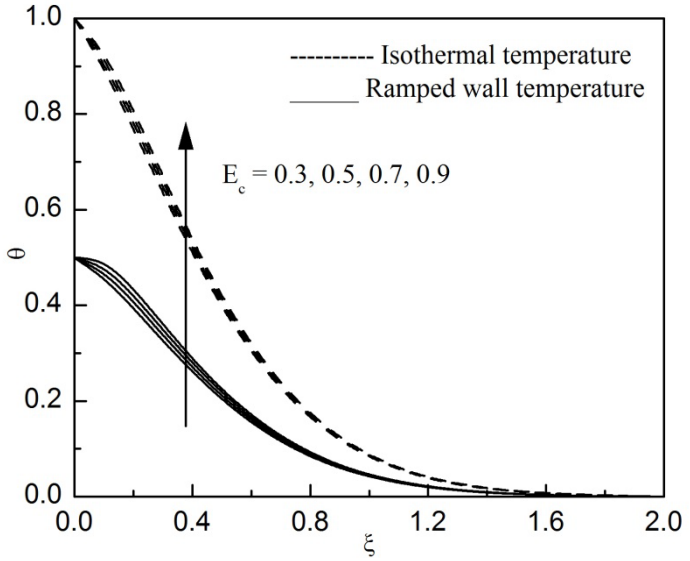

Fig.3. Temperature vs ξ for several E_c.

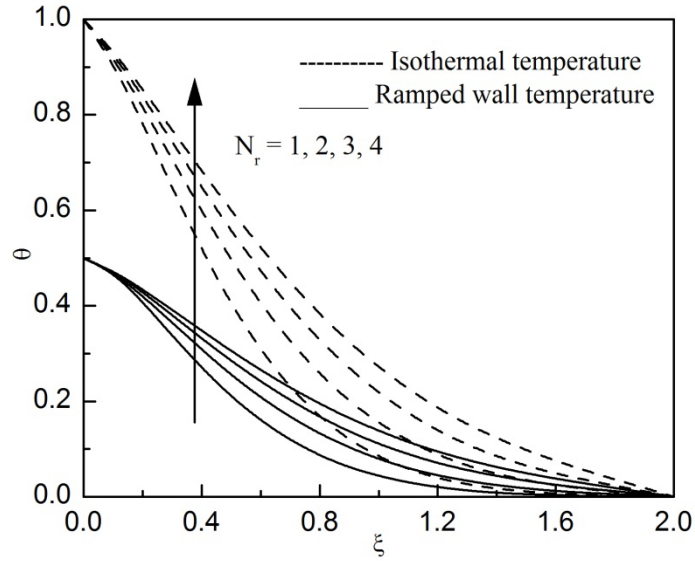

Fig.4. Temperature vs ξ for several N_r.

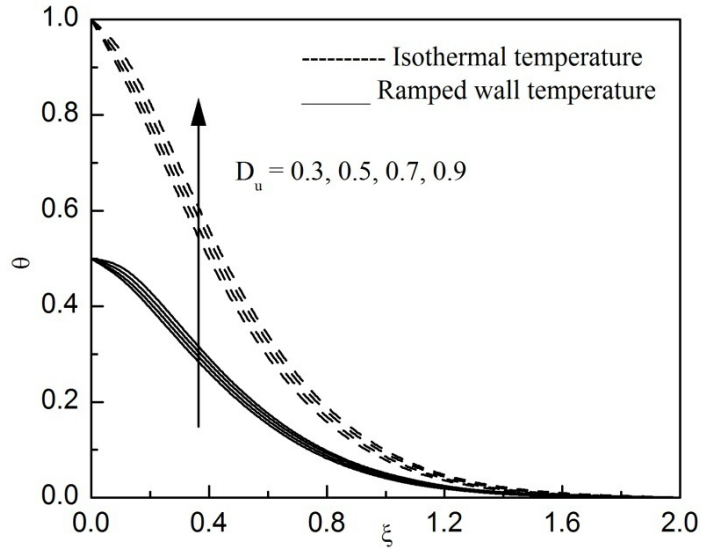

Fig.5. Temperature vs ξ for several D_u.

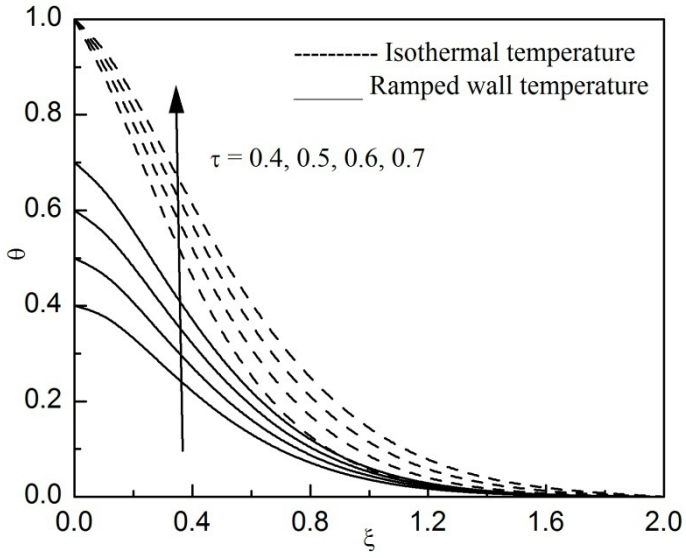

Fig.6. Temperature vs ξ for several τ.

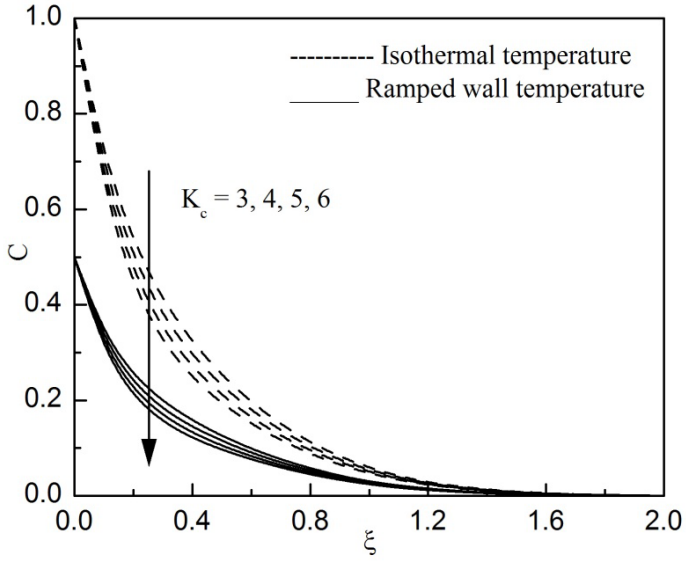

Fig.7. Concentration vs ξ for several K_c.

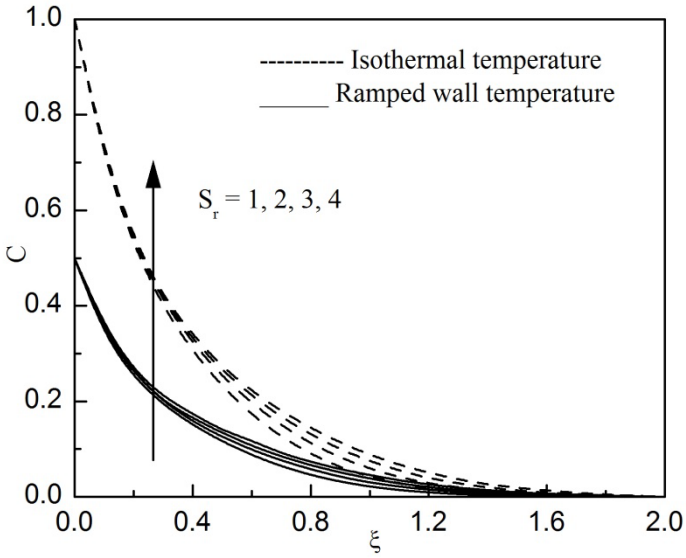

Fig.8. Concentration vs ξ for several S_r.

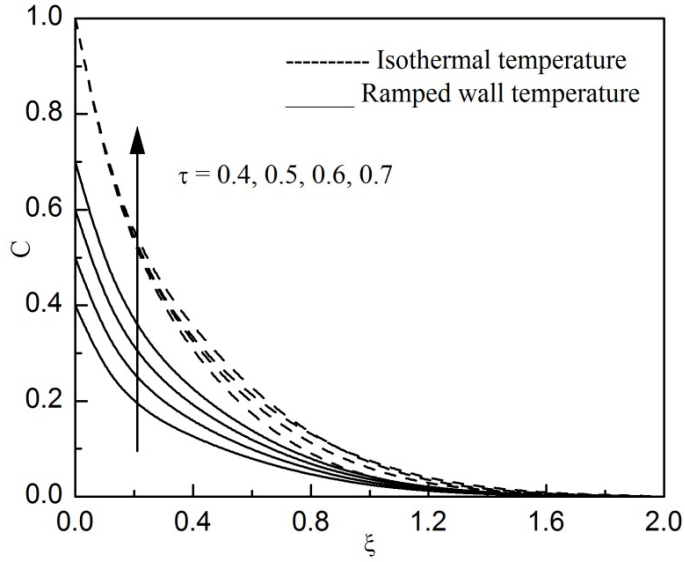

Fig.9. Concentration vs ξ for several τ.

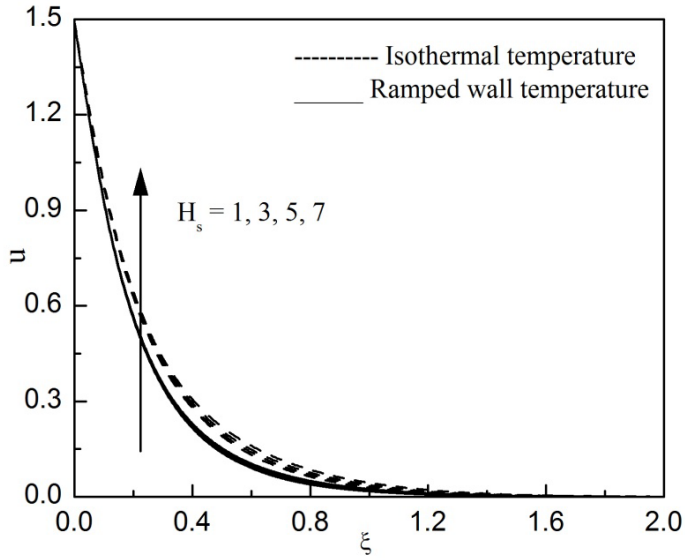

Fig.10. Velocity vs ξ for several H_s.

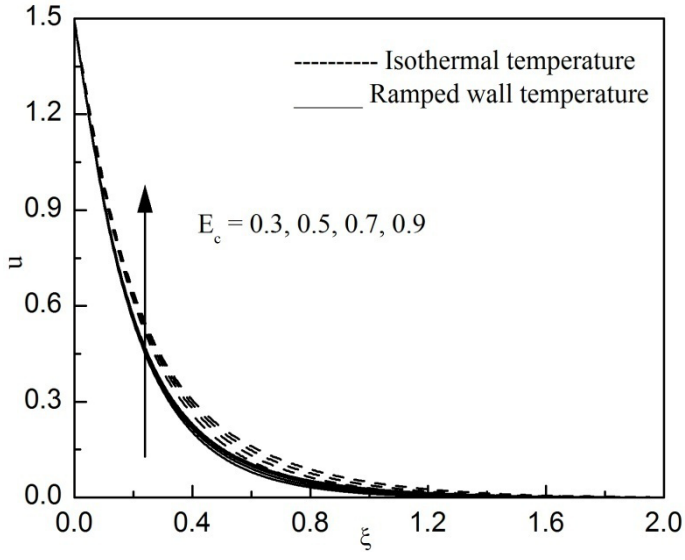

Fig.11. Velocity vs ξ for several E_c.

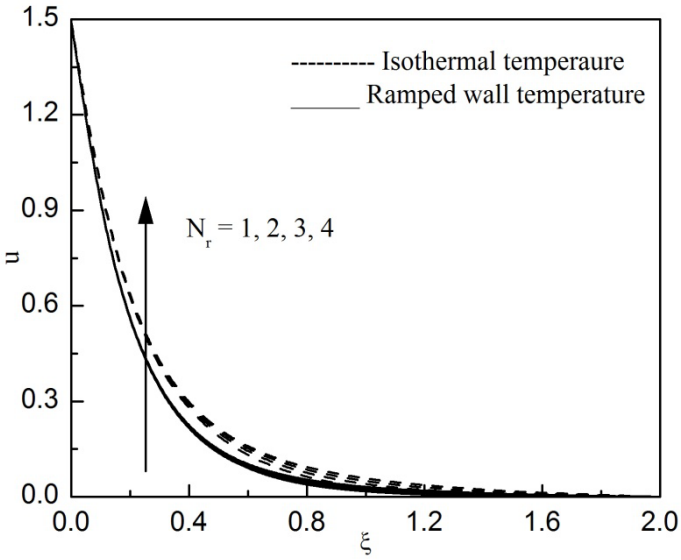

Fig.12. Velocity vs ξ for several N_r.

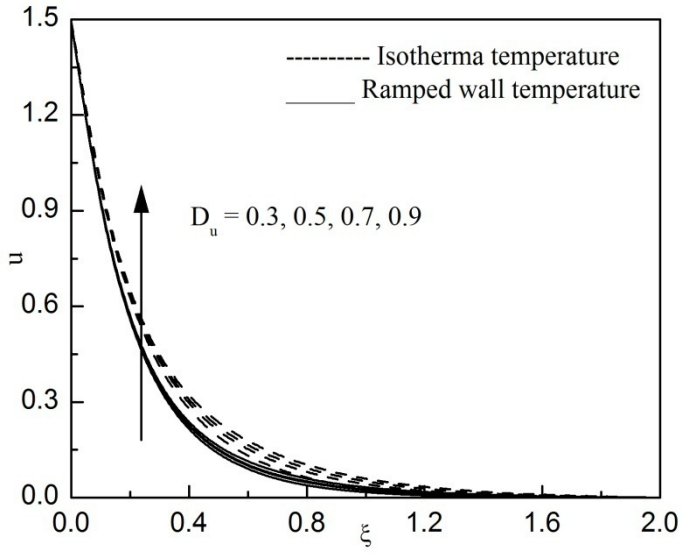

Fig.13. Velocity vs ξ for several D_u.

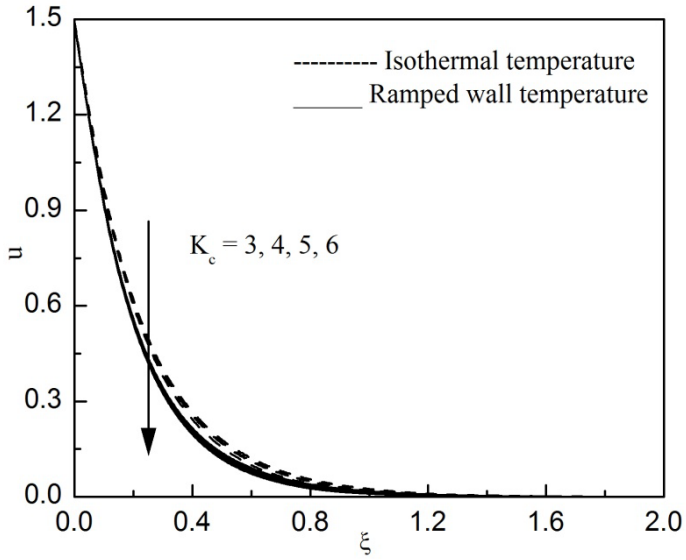

Fig.14. Velocity vs ξ for several K_c.

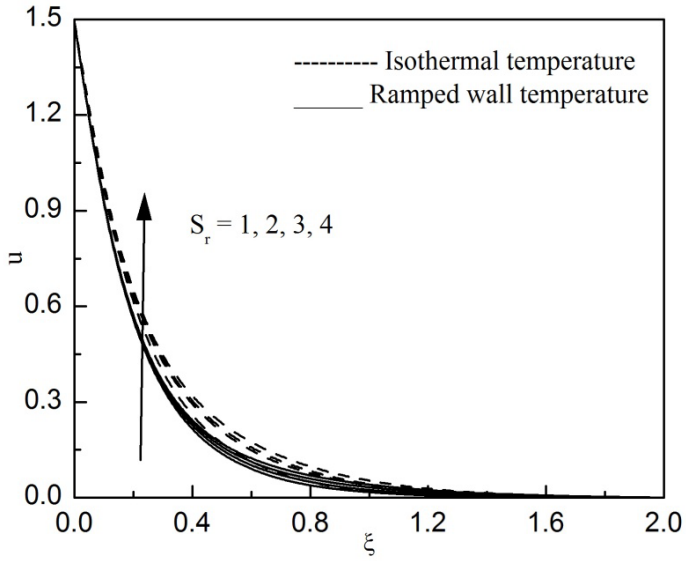

Fig.15. Velocity vs ξ for several S_r.

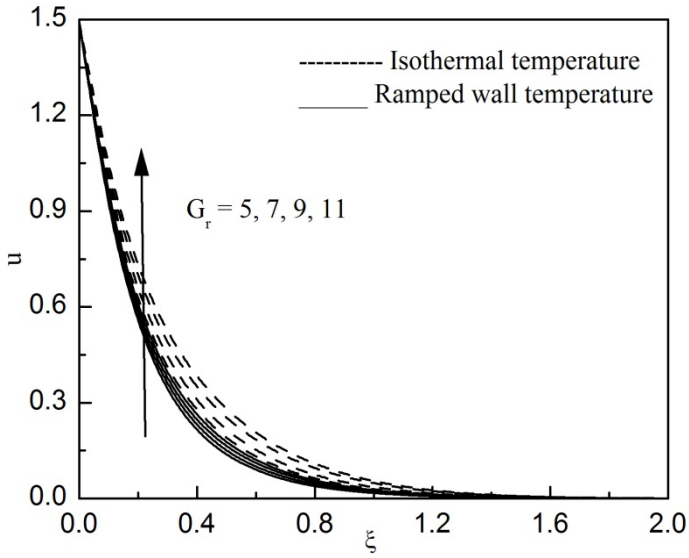

Fig.16. Velocity vs ξ for several G_r.

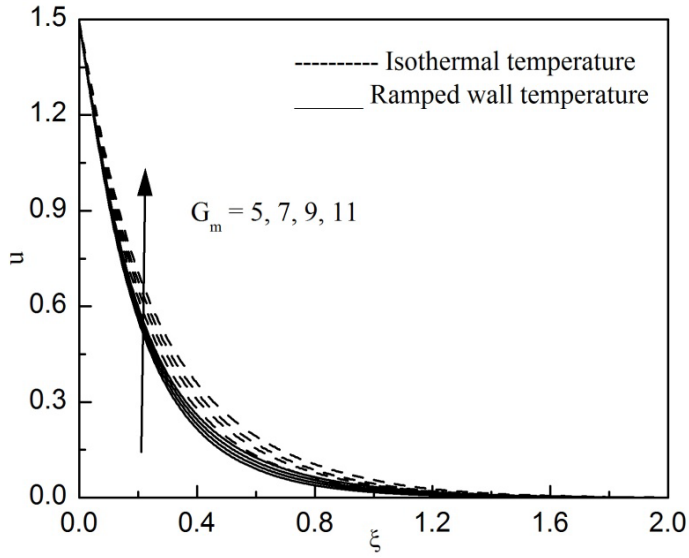

Fig.17. Velocity vs ξ for several G_m.

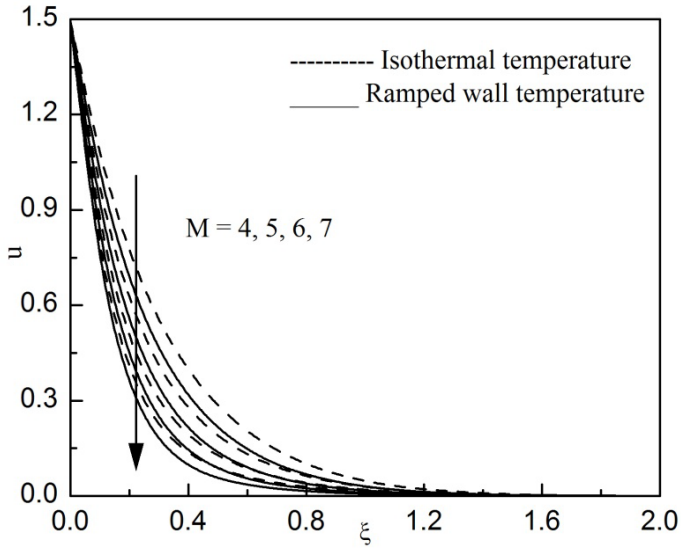

Fig.18. Velocity vs ξ for several M.

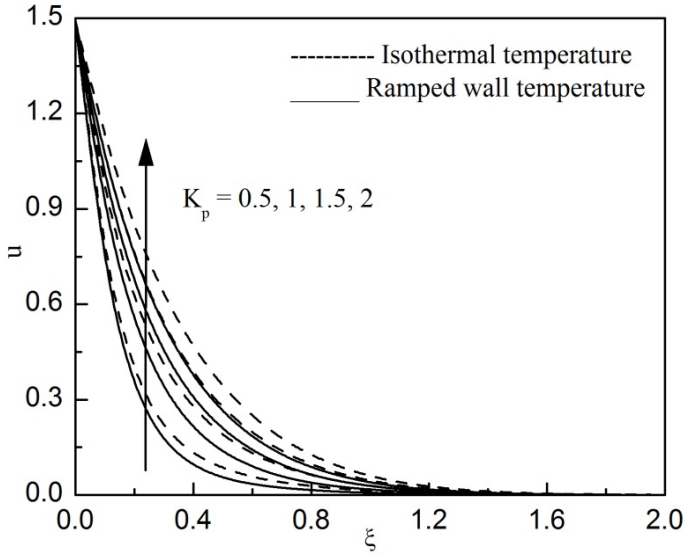

Fig.19. Velocity vs ξ for several K_p.

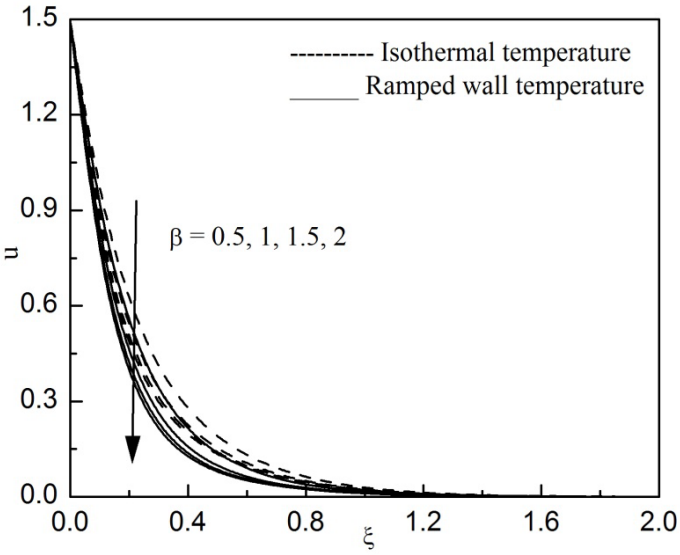

Fig.20. Velocity vs ξ for several β.

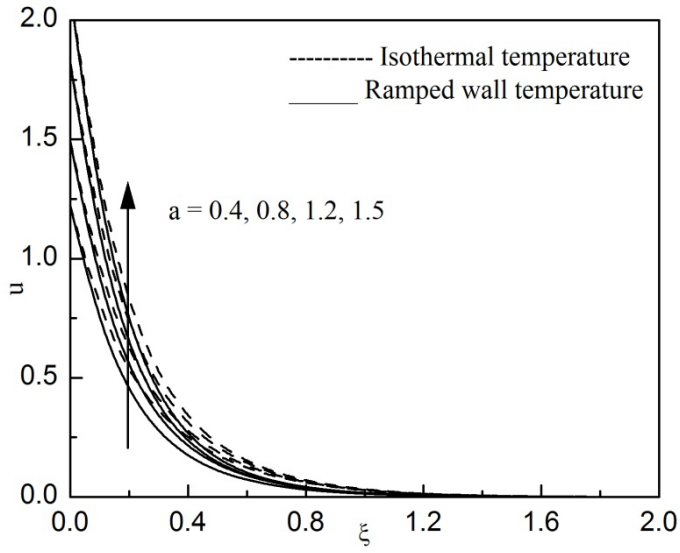

Fig.21. Velocity vs ξ for several a.

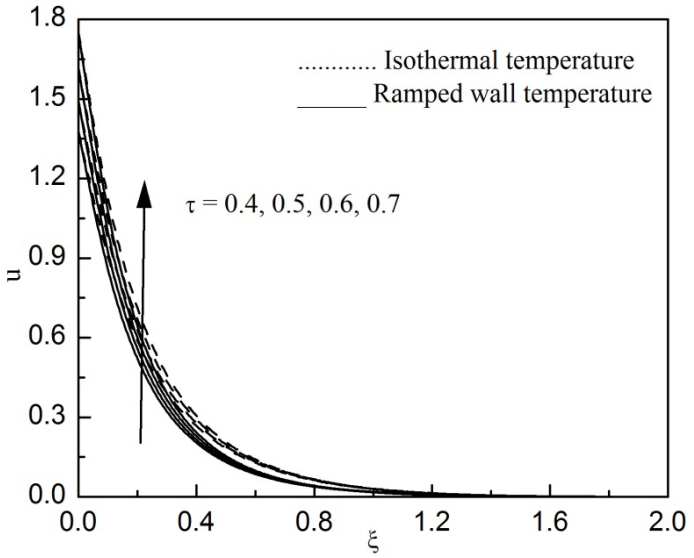

Fig.22. Velocity vs ξ for several τ.

Tables 3, 4, 5 and 6 display the numerical variation of Nusselt number N_u, Sherwood number S_h and skin friction S_f in the presence of varying flow control parameters. It is highlighted in Table 3 that in the instance of ramped and isothermal temperature, with an expanding value of N_r, H_s, D_u and E_c, the Nusselt number N_u is considerably diminished. Considering two thermal conditions, we observe form Table 4 that a diminution effect in the Sherwood number S_h with increased thermo-diffusion parameter S_r whereas an opposite effect is perceived in the Sherwood number S_h with augmented chemical reaction parameter K_c. From Tables 3 and 4, we conclude that the rising time τ causes to decrease both N_u and S_h for ramped temperature, and the opposite result is observed for isothermal temperature. Further, it can be seen from Table 4 that our numerically computed results of S_h are precisely matching with the analytically computed results of Nandi and Kumbhakar (2021), which demonstrate the accuracy of the current numerical method. Tables 5 and 6 displayed that, for two considered thermal conditions, the skin friction τ intensifies with alteration of M, β, γ, a and τ whereas the opposite trend is noticed with respect to H_s, E_c, D_u, G_r, G_m, N_r, K and S_r.

N_r	H_s	D_u	E_c	τ	N_u

					Ramped	Isothermal
1	1	0.5	0.5	0.5	0.258830	0.358612
2					0.241027	0.314920
3					0.215980	0.285472
1	3				0.195025	0.251404
	5				0.158000	0.136708
	1				0.194430	0.293464
		0.7			0.178387	0.217516
		0.9			0.167310	0.302180
		0.5	0.7		0.140461	0.265876
			0.9		0.410478	0.287972
			0.5	0.6	0.532060	0.229612
				0.7		

Table 3. Numerical variation of N_u.

S_r	K_c	τ	Nandi and Kumbhakar (2021)		Current results	
			Ramped	Isothermal	Ramped	Isothermal
0.5	0.2	0.20	0.23044	0.61442	0.230445	0.614428
2.0			0.20226	0.61197	0.202269	0.611970
4.0			0.16469	0.60870	0.164691	0.608709
0.5	1.0		0.24307	0.70740	0.243070	0.707405
	1.5		0.25076	0.76308	0.250764	0.763088
	0.2	0.10	0.16027	0.82784	0.160274	0.827840
		0.15	0.19792	0.69254	0.197921	0.692542

Table 4. Sherwood number S_h.

β	K_p	M	G_r	G_m	N_r	S_f	
						Ramped	Isothermal
0.5	1	5	5	5	1	2.428848	1.561147
1.0						2.806032	1.685695
1.5						2.985601	1.743230
0.5	1.5					2.014708	1.102905
	2					1.755616	0.926940
	1	6				2.841100	1.660852
		7				3.212080	1.909012
		5	7			2.377488	1.321412
			9			2.226152	1.249347
			5	6		2.107104	1.491940
				7		1.845704	1.466065
				5	2	1.964172	1.377827
					3	1.683871	1.297396

Table 5. Numerical variation of S_f when $E_c = 0.5, H_s = 1, D_u = 0.5, S_r = 2, K_c = 2,$ $a = 0.8$ and $\tau = 0.5$.

							S_f

E_c	H_s	D_u	S_r	K_c	a	τ	Ramped	Isothermal
0.5	1	0.5	2	3	0.8	0.5	2.428848	1.561147
0.7							1.895928	1.370650
0.9							1.721982	1.106127
0.5	3						2.123764	1.277162
	5						1.992656	1.096978
	1	0.7					2.113344	1.367930
		0.9					2.021948	1.303005
		0.5	3				1.702894	1.407111
			4				1.657928	1.263350
			2	4			2.517011	1.705322
				5			2.602914	1.811655
				3	1.2		2.751520	1.748815
					1.5		2.901011	2.050321
					0.8	0.6	2.648884	2.119757
						0.7	2.887280	2.504286

Table 6. Numerical variation of S_f when $\beta = 0.5, K_p = 1, M = 5, G_r = 5, G_m = 5$ and $N_r = 1$.

5. Conclusions

The developed physical model has been numerically simulated by the efficient finite difference technique to examine the description of raditive mixed convection heat forming unsteady non-Newtonian Casson reactive dissipating fluid passing across an exponentially stimulant vertical porous plate with Dufour-Soret effect in existing of ramped temperature and concentration. The significant findings of the research are as follows.

i. The fluid velocity and temperature intensifies with magnification of E_c, N_r, H and D_u but these parameters have reversal propensity on S_f and N_u for both thermal conditions.

ii. Increased M and β caused a decrease of the fluid velocity, but rising G_r, G_m and K showed the opposite effects. These parameters have the opposite effect on S_f with respect to that of fluid velocity.

iii. The enlargement of a and τ, for both thermal conditions, S_f increases.

iv. Increasing S_r values cause a raise S_h but a reverse tendency is detected with K_c.

v. Both N_u and S_h increase with expanding τ values for ramp temperature but the contrary effect is detected for isothermal plate temperature.

vi. The fluid velocity, temperature and concentrations have larger effects to isothermal temperature than ramp surface temperature.

References:

Brewster M. Q (1972). *Thermal radiative transfer and properties*, John Wiley and Sons.

Casson N (1959). A flow equation for pigment oil suspensions of the printing ink in rheo-logy of disperse systems. Mill CC (Ed) Pergamon Press, Oxford, 84-102.

Das M, Mahato R, Nandkeolyar R (2015). Newtonian heating effect on unsteady hydro-magnetic Casson fluid flow past a flat plate with heat and mass transfer. Alexandria Engineering Journal, 54(4), 871-879.

Das M, Mahanta G, Shaw S, Parida S. B (2019). Unsteady MHD chemically reactive double-diffusive Casson fluid past a flat plate in porous medium with heat and mass transfer. Heat Transfer- Asian Research, 48(4), 1-17.

El-Kabeir S. M. M, Modathar M, Rashed A. M (2013). Soret and Dufour effects on heat and mass transfer from a continuously moving plate embedded in porous media with temperature dependent viscosity and thermal conductivity. Journal of Modern Methods in Numerical Mathematics, 4(2), 10–22.

Endalew M. F (2021). Analytical study of heat and mass transfer effects on unsteady Casson fluid flow over an oscillating plate with thermal and solutal boundary conditions. Heat Transfer, 1-15.

Ferdows M, Shamshuddin MD, Zaimi K (2020). Dissipative radiative micro-polar fluid transport in a non-Darcy porous medium with cross-diffusion effects, CFD Letters, 12 (7), 70-89.

Gopal D, Kishan N, Raju C. S. K (2017). Viscous and Joule's dissipation on Casson fluid over a chemically reacting stretching sheet with inclined magnetic field and multiple slips, Informatics Medicine, Unlocked, 9, 154–160.

Hussanan A, Salleh MZ, Tahar RM, Khan I (2014). Unsteady boundary layer flow and heat transfer of a Casson fluid past an oscillating vertical plate with Newtonian heating. Plos One, 9(10); e108763.

Hayat T, Rafiq Q. M, Alsaadi F, Ayub M (2016). Soret and Dufour effects on peristaltic transport in curved channel with radial magnetic field and convective conditions, Journal of Magnetism and Magnetic Materials, 405, 358-369.

Hussanan A, Salleh M. Z, Khan I, Tahar, R. M (2017). Heat transfer in magneto-hydrodynamic flow of a Casson fluid with porous medium and Newtonian heating. Journal of Nanofluid, 6(1), 1-10.

Hayat T, Zahir H, Tanveer A, Alsaedi A (2018). Soret and Dufour effects on MHD peristaltic flow of Prandtl fluid in rotating channel. Results in Physics, 8, 1291-1300.

Ibrahim S. M, Lorenzini G, Kumar P. V, Raju C. S. K (2017). Influence of chemical reaction and heat source on dissipative MHD mixed convection flow of a Casson nanofluid over a nonlinear permeable stretching sheet. International Journal of Heat and Mass Transfer, 111, 346–355.

Khalid A, Khan I, Khan A, Shafie S (2015a). Unsteady MHD free convection flow of Casson fluid past over an oscillating vertical plate embedded in a porous medium. Engineering Science Technology: International Journal, 18, 309-317.

Khalid A, Khan I, Shafie S (2015b). Exact solutions for unsteady free convection flow of Casson fluid over an oscillating vertical plate with constant wall temperature, Abstract and Applied Analysis, 26,1-8

Kataria H. R, Patel H. R (2016a). Radiation and chemical reaction effects on MHD Casson fluid flow past an oscillating vertical plate embedded in porous medium. Alexandria Engineering Journal, 55, 583-595.

Kataria H. R, Patel H. R (2016b). Soret and heat generation effects on MHD Casson fluid flow past an oscillating vertical plate embedded through porous medium, Alexandria Engineering Journal, 55 (3), 2125–2137.

Kataria H. R, Patel H. R (2018). Heat and mass transfer in magneto-hydrodynamic (MHD) Casson fluid flow past over an oscillating vertical plate embedded in a porous medium with ramped wall temperature. Propulsion and Power Research, 7(3), 257-267.

Kataria H. R, Patel H. R (2019). Effects of chemical reaction and heat generation/absorption on MHD Casson fluid flow over an exponentially accelerated vertical plate embedded in a porous medium with ramped wall temperature and ramped surface concentration. Propulsion and Power Research, 8(1), 35-46.

Kaladhar K, Komuraiah E, Reddy K. M (2019). Soret and Dufour effects on chemically reacting mixed convection flow in an annulus with Navier slip and convective boundary conditions. Applied Mathematics Nonlinear Science, 4(2), 475–488.

Mohamed, EI-aziz Abd Yahya, A. S (2017). Perturbation analysis of unsteady boundary layer slip flow and heat transfer of Casson fluid past a vertical permeable plate with Hall current. Applied Mathematics and Computation, 307, 146-164.

Nandi S, Kumbhakar B (2021). Hall current and thermo-diffusion effects on magneto-hydrodynamic convective flow near an oscillatory plate with ramped type thermal and solutal boundary conditions. Indian Journal of Physics, DOI: 10.1007/s12648-020-02001-0.

Prabhakar Reddy B, Ananad Rao J (2011). Radiation and thermal diffusion effects on an unsteady MHD free convection mass transfer flow past an infinite vertical porous plate with Hall current and heat source. Journal of Engineering Physics and Thermo-Physics, 84(6), 1369 – 1378.

Pal D, Vajravelu K, Mandal G (2014). Convective-radiation effects on stagnation point flow of nanofluid over a stretching surface with viscous dissipation. Journal of Mechanics, 3(30), 289-297.

Prabhakar Reddy B (2016). Mass transfer effects on an unsteady MHD free convective flow of an incompressible viscous dissipative fluid past an infinite vertical porous plate. International Journal of Applied Mechanics and Engineering, 21 (1), 143-155.

Pal D, Mandal G, Vajravalu K (2016). Soret and Dufour effects on MHD convective-radiative heat and mass transfer of nanofluid over a vertical nonlinear stretching/shrinking sheet. Applied Mathematics and Computation, 287-288(1):184-200

Prabhakar Reddy B, Sunzu J. M (2018). Dufour and Soret effects on unsteady MHD free convective flow of viscous incompressible fluid past an infinite vertical porous plate in the presence of radiation. Journal of Serbian Society for Computational Mechanics, 12(1), 9-26.

Prabhakar Reddy B (2019). Effects of chemical reaction on transient MHD flow with mass transfer past an impulsively fixed infinite vertical plate in the presence of thermal radiation. International Journal of Applied Mechanics and Engineering, 24(4), 169-182.

Patel H. R (2019). Effects of heat generation, thermal radiation and Hall current on MHD Casson fluid flow past an oscillating plate in porous medium. Multiphase Science and Technology, 31(1), 87-107.

Prabhakar Reddy B, Makinde O. D (2021). Numerical study on MHD radiating and reacting unsteady slip flow past a vertical permeable plate in a porous medium. International Journal of Ambient Energy, DOI: 10.1080/01430750.2021.1999323.

Prabhakar Reddy B, Makinde O. D (2022). Newtonian heating effect on heat absorbing unsteady radiating and chemically reacting free convection flow past an oscillating vertical porous plate. International Journal of Applied Mechanics and Engineering, 27(1), 168-187.

Prabhakar Reddy B, Joseph L. J (2022). A Numerical study on Newtonian heating effect on heat absorbing MHD Casson flow of dissipative fluid past an oscillating vertical porous plate. International Journal of Mathematics and Mathematical Sciences, Article ID 7987315 (16 pages),https://doi.org/10.1155/2022/7987315.

Reddy G. J. Raju R. S, Anand Rao J (2018). Influence of viscous dissipation on unsteady MHD natural convective flow of Casson fluid over an oscillating vertical plate via FEM. Ain Shams Engineering Journal, 9(4), 1907–1915.

Rajput U. S, Shamshuddin MD, Salawu S. O (2020). Thermo-solutal convective non-Newtonian radiative Casson fluid transport over a vertical plate propagated by Arrhenius kinetics with heat source/sink. Heat Transfer, 50(3), 2829-2848.

Subhakar M. J, Gangadhar K (2012). Soret and Dufour effects on MHD free convection heat and mass transfer flow over a stretching vertical plate with suction and heat source/sink. International Journal Modern Engineering Research, 2 (5), 3458–3468.

Seth G. S, Hussain S. M, Sarkar S (2015). Hydro-magnetic natural convection flow with heat and mass transfer of a chemically reacting and heat absorbing fluid past an accelerated moving vertical plate with ramped temperature and ramped surface concentration through a porous medium. Journal of Egyptian Mathematical Society, 23, 197-207.

Singh K, Kumar M (2016). Effect thermal radiation on mixed convection flow of micro-polar fluid from an unsteady stretching surface with viscous dissipation and heat generation/absorption. International Journal of Chemical Engineering, 4, 1-10.

Shamshuddin MD, Thirupathi T (2017). Soret and Dufour effects on unsteady MHD free convective flow of micro-polar fluid with oscillatory plate velocity considering viscous dissipation effects. Journal of Teknlogi, 79(4), 123-136.

Sreedevi G, Rao D, Prasad R. V, Makinde O. D, Reddy G. V (2017). Soret and Dufour effects on MHD flow with heat and mass transfer past a permeable stretching sheet in presence of thermal radiation. Indian Journal of Pure and Applied Physics, 55(8), 551-563.

Shamshuddin MD, Chamkha A. J, Thirupathi T, Raju M. C (2018). Computation of unsteady MHD mixed convective heat and mass transfer in dissipative reactive micro-polar flow considering Soret and Dufour effects. Frontiers in Heat and Mass Transfer, 10, DOI: 10.5098/hmt.10.15.

Shamshuddin MD, Thumma T Mishra S. R (2019). Chemically reacting radiative Casson fluid flow over an inclined plate: A numerical study. Lecture notes in Mechanical Engineering, Springer (Singapore).

Seth G. S, Bhattacharya A, Kumar R, Mishra M. K (2019). Modeling and numerical simulation of hydro-magnetic natural convection Casson fluid flow with *n*-th order chemical reaction and Newtonian heating in porous medium. Journal of Porous Media, 22(9), 1141-1157.

Ullah I, Tawfeeq A. A, Shafie S, Nisar K. S, Khan I, Makinde O. D (2019). MHD slip flow of Casson fluid along a nonlinear permeable stretching cylinder saturated in a porous medium with chemical reaction, viscous dissipation, and heat generation/absorption. *Symmetry, 11*(4), 531.

Venkateshwarlu M, Ramana Reddy G. V, Laxmi D. V (2013). Effects of chemical reaction and heat generation on MHD boundary layer flow of a moving vertical plate with suction and viscous dissipation. Engineering International, 1(1), 27-38.

Veeresh C, Raju M. C, Varma S. V. K, Vijaya Kumar A. G (2019). Effects of thermal diffusion and radiation on magneto-hydrodynamic (MHD) chemically reacting fluid flow past a vertical plate in a slip flow regime. Journal of Applied and Computational Mechanics, 5(2), 334-343.